

Multilayered PdSe₂/Perovskite Schottky Junction for Fast, Self-Powered, Polarization-Sensitive, Broadband Photodetectors, and Image Sensor Application

Long-Hui Zeng, Qing-Ming Chen, Zhi-Xiang Zhang, Di Wu, Huiyu Yuan, Yan-Yong Li, Wayesh Qarony, Shu Ping Lau, Lin-Bao Luo, and Yuen Hong Tsang*

Group-10 transition metal dichalcogenides (TMDs) with distinct optical and tunable electrical properties have exhibited great potential for various optoelectronic applications. Herein, a self-powered photodetector is developed with broadband response ranging from deep ultraviolet to near-infrared by combining FA_{1-x}Cs_xPbI₃ perovskite with PdSe₂ layer, a newly discovered TMDs material. Optoelectronic characterization reveals that the as-assembled PdSe₂/perovskite Schottky junction is sensitive to light illumination ranging from 200 to 1550 nm, with the highest sensitivity centered at ≈800 nm. The device also shows a large on/off ratio of ≈10⁴, a high responsivity (*R*) of 313 mA W⁻¹, a decent specific detectivity (*D*^{*}) of ≈10¹³ Jones, and a rapid response speed of 3.5/4 μs. These figures of merit are comparable with or much better than most of the previously reported perovskite detectors. In addition, the PdSe₂/perovskite device exhibits obvious sensitivity to polarized light, with a polarization sensitivity of 6.04. Finally, the PdSe₂/perovskite detector can readily record five “P,” “O,” “L,” “Y,” and “U” images sequentially produced by 808 nm. These results suggest that the present PdSe₂/perovskite Schottky junction photodetectors may be useful for assembly of optoelectronic system applications in near future.

including light-emitting diodes,^[6,7] lasers,^[8,9] solar cells,^[10] and photodetectors.^[11,12] Among these optoelectronic devices, photodetectors are of great importance for their promising applications in both fundamental science and industrial fields, such as image sensing, optical communication, night-vision, and environmental monitoring.^[13–15] To date, a number of emerging perovskite materials have been extensively explored for various photodetector device applications.^[4,16–18] For example, Song and co-workers reported the large-scale fabrication of CH₃NH₃PbI₃ nanowires (NWs) by a one-step self-assembly approach. The as-assembled CH₃NH₃PbI₃ NWs photodetector exhibited a responsivity of 1.32 A W⁻¹ and a specific detectivity of 2.5 × 10¹² Jones, with a response time of 0.3 ms.^[19] Additionally, Deng et al. developed highly sensitive perovskite photodetectors made of high-quality single-crystalline aligned CH₃NH₃PbI₃ microwire arrays through

facile blade coating approach. The resulting micro-photodetectors showed broadband sensitivity with peak responsivity (13.57 A W⁻¹) and detectivity (5.25 × 10¹² Jones) under 420 nm light illumination. What is more, the rise and fall time were calculated to be 80 and 240 μs, respectively.^[20] Despite these great achievements, it is undeniable that most of the perovskite photodetectors are often characterized by low specific detectivity and slow photoresponse, which inevitably limit their practical applications, especially in high-capacity networks, high-speed

1. Introduction

Organic/inorganic halide perovskite materials have in the past decade stimulated broad research interest for their excellent optoelectronic properties including long diffusion length, low trapping density, large absorption coefficient, and multiband light absorption.^[1–5] With these distinct properties, this group of hybrid halide materials has demonstrated great potential as building blocks for assembly of various optoelectronic devices,

L.-H. Zeng, Dr. Q.-M. Chen, Dr. H. Yuan, Dr. Y.-Y. Li, W. Qarony, Prof. S. P. Lau, Prof. Y. H. Tsang
Department of Applied Physics
The Hong Kong Polytechnic University
Hung Hom, Kowloon, Hong Kong 999077, China
E-mail: yuen.tsang@polyu.edu.hk

 The ORCID identification number(s) for the author(s) of this article can be found under <https://doi.org/10.1002/adv.201901134>.

© 2019 The Authors. Published by WILEY-VCH Verlag GmbH & Co. KGaA, Weinheim. This is an open access article under the terms of the Creative Commons Attribution License, which permits use, distribution and reproduction in any medium, provided the original work is properly cited.

DOI: 10.1002/adv.201901134

Z.-X. Zhang, Prof. L.-B. Luo
School of Electronic Science and Applied Physics
Hefei University of Technology
Hefei, Anhui 230009, China

Dr. D. Wu
School of Physics and Engineering and Key Laboratory of Material Physics of Ministry of Education
Zhengzhou University
Zhengzhou, Henan 450052, China

telecommunication, and fast imaging.^[4,21] To address the above issues, a number of new device geometries that are fabricated by combining perovskite and other materials (e.g., PbSe quantum dots^[22] graphene,^[4] and black phosphorus^[23]) have been proposed, which proves to be an excellent strategy to improve the perovskite based detectors performance.^[24]

As a new material family, 2D layered transition metal dichalcogenides (TMDs) materials have shown great potential for electronics and optoelectronics applications due to their unique thickness-dependent properties, high carrier mobility, and good air stability.^[25–27] Owing to these outstanding properties, 2D layered TMDs (e.g., MoS₂,^[16] WS₂,^[28] and PtSe₂^[29]) have been successfully integrated with perovskite to achieve high-performance photodetectors including photoconductor, phototransistor, and photodiode. By virtue of synergistic effect, these detectors exhibited enhanced photoconductive gain and photoresponsivity. Enlightened by the above works, we developed a high-performance Schottky junction photodetector by combining Cs-doped FAPbI₃ perovskite with multilayer PdSe₂, a newly explored 2D layered group-10 TMDs, which has been widely applied in solar cells, field-effect transistors, and photodiodes.^[30–32] Such a PdSe₂/Cs-doped FAPbI₃ perovskite offers obvious advantages in the following three aspects: i) Compared with other 2D materials like black phosphorus, the wafer-scale and uniform PdSe₂ films with precise layer numbers can be synthesized on arbitrary substrates in low temperature, which renders the easy fabrication of large-area integrated devices. ii) It has been theoretically reported that 2D PdSe₂ exhibits high carrier mobility more than 1000 cm² V⁻¹ s⁻¹,^[33–35] resulting in fast photoresponse.^[29] iii) Significantly, its low-symmetry crystal structure endows PdSe₂ based device with good capability to detect polarized light signal.^[33] It is revealed that the as-assembled PdSe₂/perovskite device exhibits obvious photovoltaic behavior, which enables it to function as a self-powered photodetector for detecting light over broadband wavelength region from 200 to 1550 nm. Under 808 nm light illumination, the device achieves impressive device performance in terms of a large on/off ratio of ≈10⁴, a high responsivity (*R*) of 313 mA W⁻¹, a decent specific detectivity (*D*^{*}) of ≈10¹³ Jones, a high polarization sensitivity of 6.04, as well as a fast response speed of 3.5/4 μs. These results suggest that the present device may find potential application in future optoelectronic devices and systems.

2. Results and Discussion

Figure 1a shows the schematic illustration of the PdSe₂ layer/perovskite Schottky junction device. In this study, the large-area, continuous, and high-quality multilayer 2D PdSe₂ films were synthesized on a SiO₂/Si substrate (300 nm SiO₂ thickness) via a simple selenization method,^[36] and the Cs-doped FAPbI₃ perovskite layer as the light absorption medium was then drop casted by spin-coating method (More details about the synthesis of PdSe₂, perovskite, and the device fabrication are provided in the Experimental Section). Due to distinct difference in contrast, both PdSe₂ layer and perovskite material can be easily distinguished from photographic device image, as shown in Figure S1a in the Supporting Information. From the cross-section transmission electron microscopy (TEM) image in Figure 1b, we

can easily find that the PdSe₂ films are multilayered structure with a thickness of about 22 nm, in consistence with the result derived from atomic force microscopy (AFM) (Figure 1c). The PdSe₂ sample crystallizes in pentagonal manner with lattice distance of 0.27 and 0.23 nm, corresponding to the (200) and (022) planes, as shown in Figure S1b in the Supporting Information.^[30,34] The chemical composition was confirmed by an energy dispersive spectroscopy analysis and X-ray photoemission spectroscopy (Figure S1c–e, Supporting Information), in which the stoichiometric ratio of Se: Pd is determined to be 2: 1. Figure 1d presents Raman spectrum of 2D PdSe₂, which consists of four obvious peaks at ≈143.2, ≈206.1, ≈223.2, and ≈257.2 cm⁻¹. The first three peaks defined as A_g¹, A_g², and B_{1g} could be ascribed to the movements of Se atoms, while the highest mode (A_g³) at the highest wavenumber is assigned to the relative movements between Se and Pd atoms.^[34,37] Further Raman intensity mapping of A_g³ mode in inset of Figure 1d shows a narrow peak intensity distribution, signifying the good uniformity and homogeneity of as-grown PdSe₂ films. To study the anisotropic property of 2D PdSe₂, the angle-resolved polarized Raman spectroscopy was measured by adjusting the analyzer to be parallel to laser polarization. As presented in Figure 1e, compared with stronger Raman peaks of A_g¹ and A_g³, the A_g² and B_{1g} peaks are too weak to be observed in the all polarized Raman spectra due to the lower excitation light intensity. Specifically, the peak intensity of A_g¹ and A_g³ mode is found to gradually decrease in the polarization angle ranging from 0° to 90° but increase when the polarization angle varies from 90° to 180°, as revealed by the anisotropy variation period of two Raman modes (A_g¹ and A_g³) in Figure S2 in the Supporting Information. According to the field emission scanning electron microscopy (FESEM) image in Figure S3a in the Supporting Information, the large-area and continuous Cs-doped FAPbI₃ perovskite films with relatively smooth surface can be easily synthesized. From the X-ray diffraction (XRD) patterns in Figure S3b in the Supporting Information, all the signals can be readily ascribed to the diffraction peaks of black phase FAPbI₃ perovskite.^[18,38]

Figure 2a plots the current–voltage (*I*–*V*) curve of device in dark. Apparently, this Schottky junction displays a conventional rectifying behavior with a rectification ratio of ≈60 at ± 5 V, which is higher than that of MoS₂/WS₂ (≈5),^[39] PtSe₂/MoS₂ (15–20),^[40] graphene/In₂S₃ (≈32),^[41] and PtSe₂/perovskite heterojunctions (≈10),^[29] but is slightly lower than that of MoS₂ p–n junction (≈67).^[42] Considering the good linear *I*–*V* characteristics for Au–PdSe₂ and Au–perovskite achieved (Figure S4, Supporting Information), the observed rectifying behavior should arise from the Schottky barrier formed at the PdSe₂/perovskite interface. Interestingly, when the device is shinned by several light sources (265, 365, 650, 808, and 980 nm) with constant light intensity of 0.3 mW cm⁻², the photocurrent at negative bias region substantially increases with increasing wavelength from 265 to 808 nm but decreases subsequently when the incident wavelength further increases to 980 nm (Figure 2b), indicative of a peak sensitivity in the region from 650 to 980 nm. Careful examination of *I*–*V* curves finds a weak photovoltaic effect under light illumination (the inset of Figure 2b). Despite relatively low energy-conversion efficiency with a short-circuit current (*I*_{sc}) of ≈2.14 μA and an open-circuit voltage (*V*_{oc}) of ≈0.3 V, the weak photovoltaic behavior can enable the present device

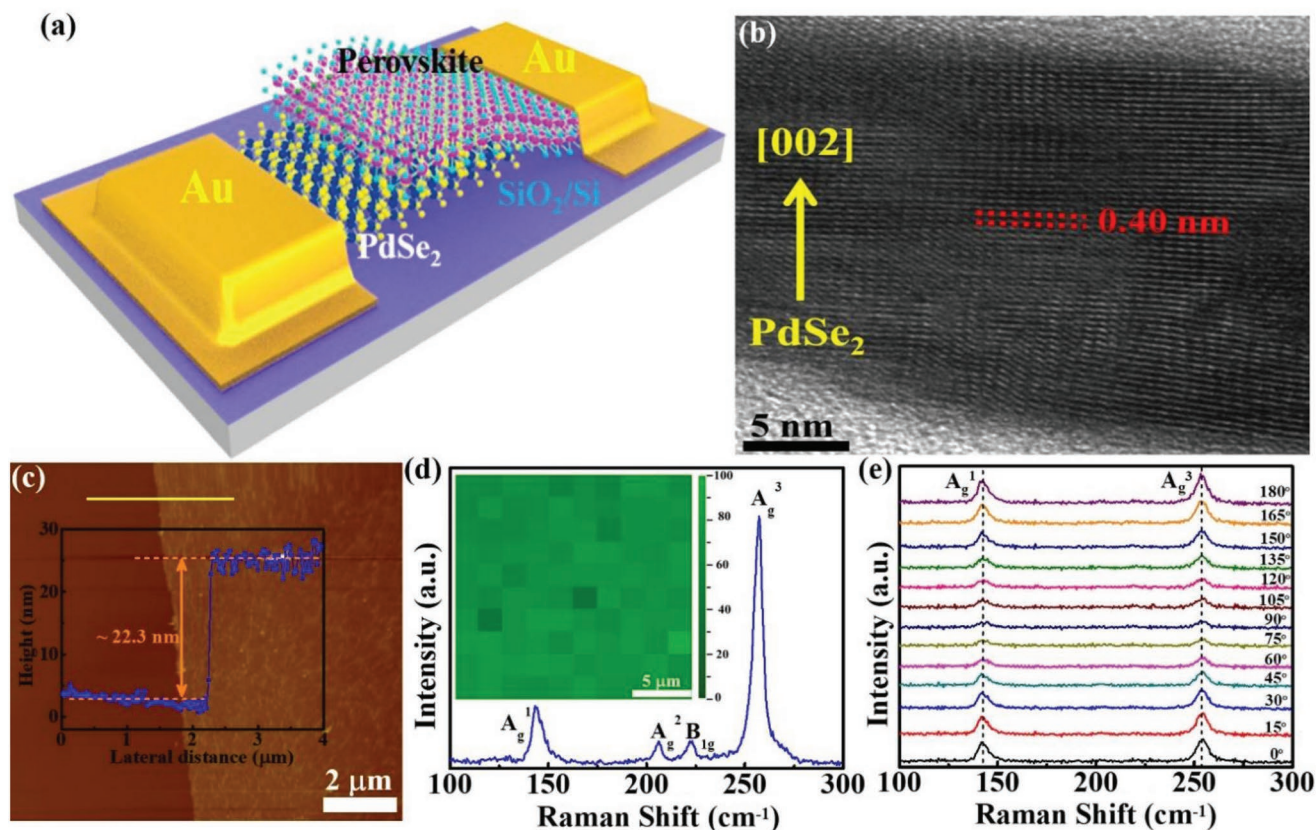


Figure 1. a) Schematic illustration of the as-fabricated PdSe₂/perovskite device. b) Typical cross-section TEM image of PdSe₂. c) AFM image and inset shows height profile. d) The Raman spectrum of PdSe₂ sample. Inset shows 2D Raman intensity mapping of A_g³ mode within 20 × 20 μm². e) Angle-resolved polarized Raman spectra of 2D PdSe₂.

to function as a self-powered photodiode operating without external bias voltage, producing obvious photoresponse in Figure 2c. Further photoresponse analysis reveals that the PdSe₂/perovskite photodiode can be easily switched between on and off states with perfect reproducibility and stability by repeatedly turning light (808 nm) on and off, even after 2000 cycles of operation, yielding a high on/off ratio of 6.46×10^4 . From the wavelength-dependent external quantum efficiency (EQE) plotted in Figure 2d, one can easily find that the device displays a good detection capability covering from 200 to 1200 nm, with the peak EQE located at ≈ 800 nm (Figure 2d), in consistency with the absorption curve shown in Figure 2h. Although the sensitivity of PdSe₂/perovskite Schottky junction was relatively weaker in the deep ultraviolet and NIR region, the device is still capable of detecting 200 nm (deep UV), 1310 nm (O band), and 1550 nm (C band) light illumination (Figure 2e–g), which are potentially important for application in both military surveillance and optical communication.^[43–45] We believe such a broadband photoresponse with good spectral selectivity is directly associated with optical absorption of hybrid PdSe₂/perovskite system. Compared with the individual absorption spectrum of perovskite on a quartz substrate (Figure 2h), the absorption spectrum of hybrid PdSe₂/FA_{0.85}CS_{0.15}PbI₃ system also covers the NIR region larger than 800 nm (the inherent cutoff optical absorption of perovskite), due to the strong absorption of PdSe₂ films in NIR region.

The photoresponse properties of Schottky junction photodiode are found to highly depend on the NIR light (808 nm) intensity. Figure 3a depicts a series of *I*–*V* curves under 808 nm light illumination with different intensities. It is obvious that the photocurrent will rise sharply at both zero and reverse bias with the increase of power intensity. Specifically, the photocurrent increases from 0.549 to 2.14 μA at 0 V with light intensity changing from 35.1 to 300.6 μW cm^{−2} (Figure 3b). Such an evolution in photoresponse is understandable given the fact that the increased population of photoexcited electron–hole pairs can lead to a monotonous increase in photocurrent under higher light intensity. The above light intensity dependent photocurrent can be described using formula of $I_{ph} \propto P^\theta$, and then θ is determined to be 0.588 ($\theta < 1$), which indicates the presence of traps and defects in photodetector.^[44,46,47] As a matter of fact, a similar evolution was observed in the dependence of on/off ratio on light intensity as well: The on/off ratio is found to increase from 1.66×10^4 to 6.46×10^4 when the light intensity ranges from 35.1 to 300.6 μW cm^{−2}.

To quantitatively evaluate the performance of Schottky junction photodetector, two representative parameters including responsivity (*R*) and specific detectivity (*D*^{*}) were determined using extensively studied equations as follows

$$R(AW^{-1}) = \frac{I_{ph}}{P_{opt}S} = \frac{I_{light} - I_{dark}}{P_{opt}S} \quad (1)$$

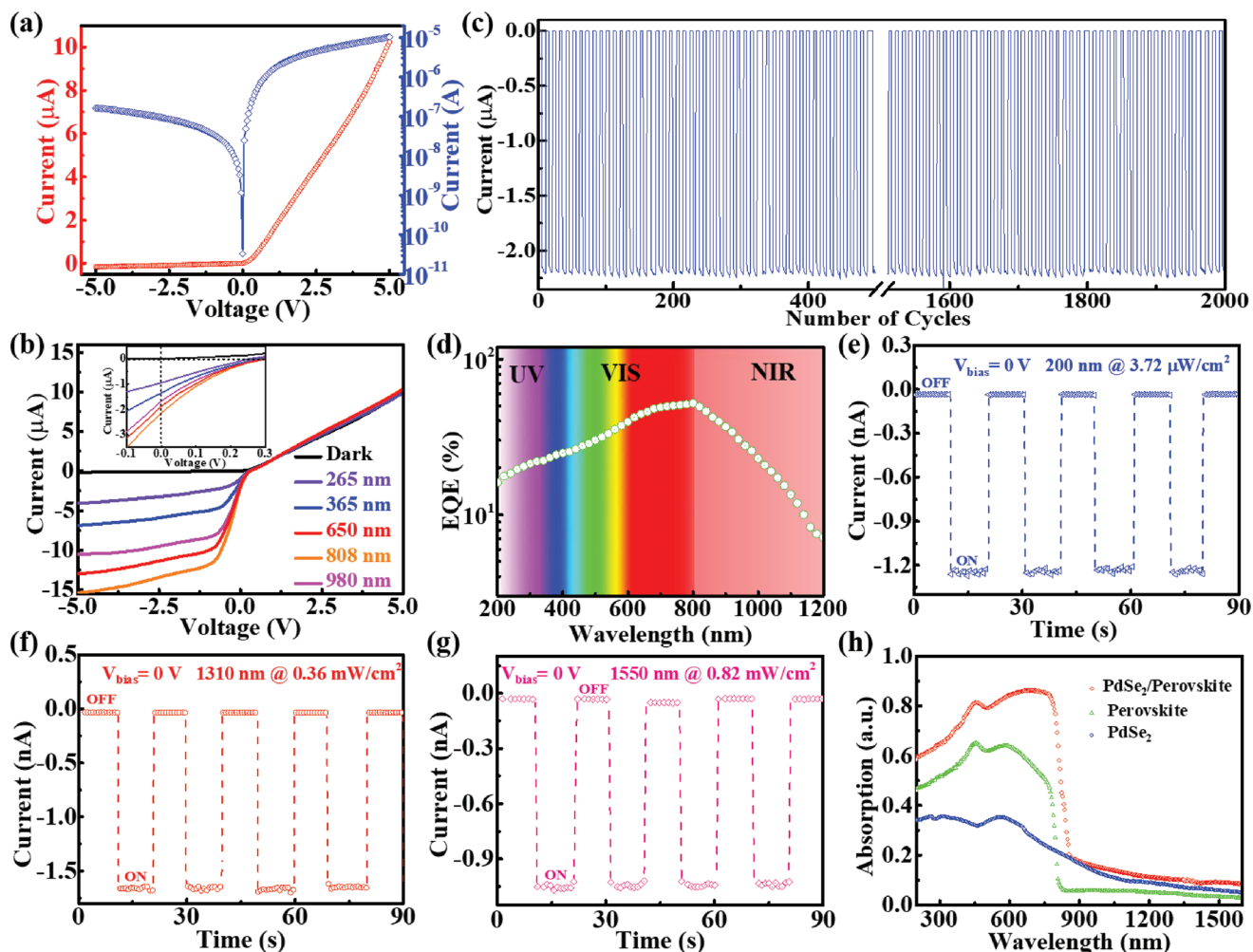


Figure 2. a) I - V curve of the PdSe₂/perovskite Schottky junction device in dark. b) I - V curve of photodetector in dark and under different light illuminations with wavelength of 265, 365, 650, 808, and 980 nm (Intensity: 0.3 mW cm⁻²), respectively. c) Time-dependent response of Schottky junction device after 2000 cycles operation. d) The wavelength-dependent external quantum efficiency (EQE) of PdSe₂/perovskite device at zero bias under the same light intensity of 10 μW cm⁻². Temporal photoresponse of Schottky junction device under e) 200 nm (3.72 μW cm⁻²), f) 1310 nm (0.36 mW cm⁻²), and g) 1550 nm (0.82 mW cm⁻²) light illuminations. h) Absorption spectrum of the PdSe₂/perovskite hybrid system. The absorption spectra of pure PdSe₂ and perovskite prepared on quartzes are also measured for comparison.

$$D^* = A^{1/2} R / (2qI_d)^{1/2} \quad (2)$$

where the net photocurrent (I_{ph}) can be determined by the difference between photocurrent (I_{light}) and dark current (I_{dark}), P_{opt} is the incident power intensity, S is the effective illuminated area (0.05 cm²), A is the effective device area (0.08 cm²), and q is the elementary electronic charge. Based on the above two equations, the R and D^* were calculated to be 313 mA W⁻¹ and 2.72×10^{13} Jones by adopting lower light intensity of 35.1 μW cm⁻² at 0 V. These values at different light intensities were plotted in Figure 3d, from which both R and D^* are found to decrease with increasing power intensity. Such decrease at high light intensity is ascribed to enhanced carrier recombination by defects.^[43,45] Actually, apart from the influence of light intensity, the photoresponse is also dependent on the operating bias voltage. As depicted in Figure 3e, as the operating voltage rises from -1 to -5 V, the photocurrent monotonously increases from 11.8 to 14.8 μA. Meanwhile, both corresponding R and

D^* values under different operating voltages were calculated and plotted in Figure 3f. One can clearly find that R increases gradually with increasing bias voltage. Such a finding is reasonable as the separation efficiency and drift velocity of the photo-generated carriers are improved by enhanced built-in electric field at reverse bias. On the contrary, the D^* is found to slightly decrease with the increase of working bias voltage owing to the significantly enhanced dark current at reverse bias. In addition to the superior photoresponse characteristics, the PdSe₂/perovskite detector also exhibits high sensitivity to polarized incident light, which is often observed in some low-dimensional nanostructure-based photodetectors.^[48,49] Figure 3g shows the testing setup of photoresponse as a function of incident light with different polarization angle, which was obtained by a homemade polarization detection test equipment (The light can pass through a polarizer to produce polarized light illuminating device). Figure 3h plots the angle-resolved normalized photocurrent curve under 808 nm light illumination at 0 V,

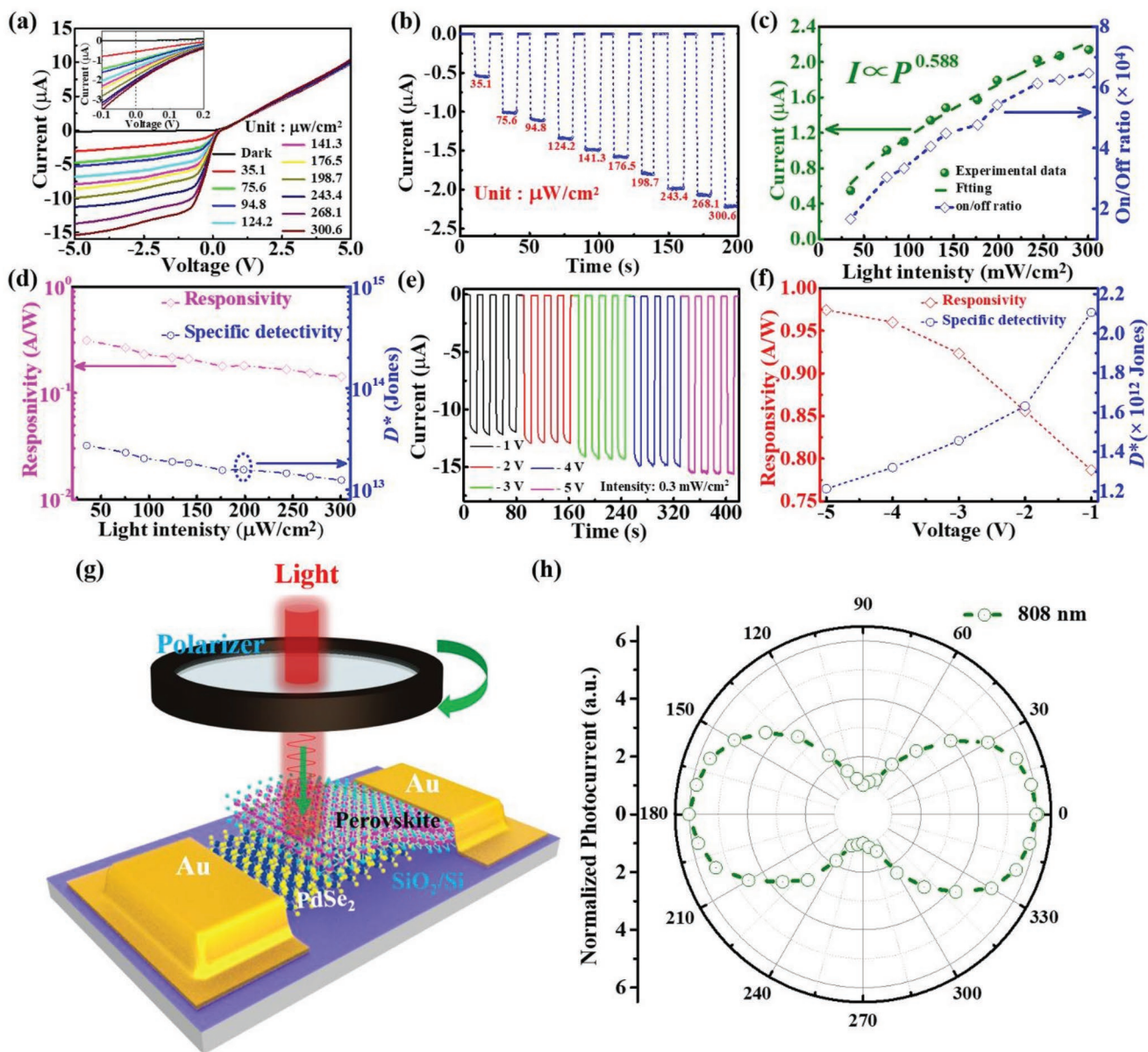


Figure 3. a) I - V curves of the PdSe₂/perovskite detector in dark and under 808 nm light irradiation with different intensities. b) The real time-dependent photocurrent of device under 808 nm light illumination with different light intensities. c) Photocurrent and on/off ratio as a function of light intensity at 0 V. d) R and D^* as a function of incident power intensity. e) The real time-dependent photocurrent of device at reverse bias under 808 nm light illumination (0.3 mW cm⁻²). f) R and D^* as a function of operating bias voltage under light intensity of 0.3 mW cm⁻². g) Schematic diagram of polarized detection device based on the PdSe₂/perovskite. h) The evolution photocurrent as a function of different polarized angle.

from which one can clearly see that the output photocurrent highly depends on polarization angle. When the polarization angle changes from 0° to 360°, the normalized photocurrent varies periodically and reaches the maximum value at 0° (180°) and minimum value at 90° (270°), with a high polarization sensitivity of 6.04. Such a high value can be directly ascribed to high-quality and strong anisotropic crystal structure of 2D PdSe₂,^[30,33] which holds potential application in optical switch, navigation, and high contrast polarizer.^[50]

The obvious photoresponse mentioned above can be explained by the energy band diagram shown in Figure 4a,b. Based on the ultraviolet photoemission spectroscopy (UPS)

analysis in Figure S5a in the Supporting Information, the multilayer PdSe₂ is semimetal with work function of ≈5.12 eV. In addition, according to the photoluminescence (PL) spectrum (Figure S5b, Supporting Information), the bandgap of the perovskite is estimated to be ≈1.55 eV. By combining with UPS results in Figure S5c in the Supporting Information, the Fermi level, bottom level of conduction band, and onset of valence band of FA_{0.85}CS_{0.15}I₃ are determined to be at ≈4.57 eV, ≈3.9 eV, ≈5.45 eV, indicating a weak n -type semiconducting characteristic.^[18,21] Once the perovskite and PdSe₂ are in contact, owing to the difference in Fermi level, the electrons would move from the perovskite to the PdSe₂ until both Fermi levels align,

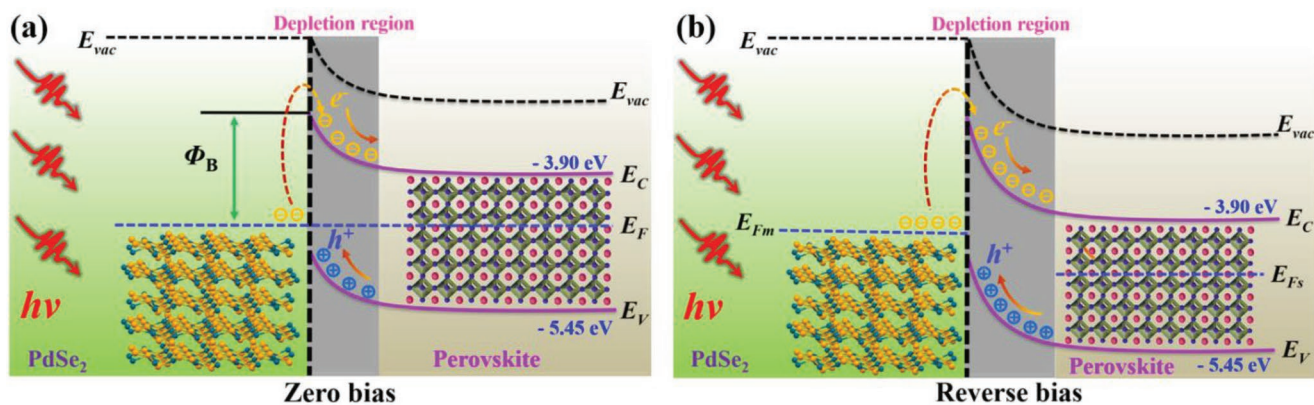


Figure 4. Energy band diagram of PdSe₂/perovskite Schottky junction under a) zero and b) reverse bias.

leading to the bending upward of energy levels and the formation of built-in potential at the interface of PdSe₂/perovskite. As illustrated in Figure 5a, when the photon energy for incident light is larger than the bandgap of perovskite ($E_g = 1.55$ eV), the light will be absorbed by both perovskite and PdSe₂ films, the resultant electron-hole pairs will be excited and then quickly separated by the built-in potential, give rising to photocurrent.^[29] For the photons with energy between bandgap of perovskite (wavelength >800) and Schottky junction barrier ($\Phi_B < h\nu < E_g$), the PdSe₂ films will mainly absorb the light. Electrons generated from PdSe₂ will overcome contact barrier and move to the perovskite, which endows the PdSe₂/perovskite

device with ability to detect the NIR light with wavelength up to 1550 nm. As a matter of fact, the depletion region could be further broadened by reverse bias, allowing the larger population of photoexcited carriers to generate higher photocurrent. The lower PL intensity of the hybrid PdSe₂/perovskite system also suggests the efficient separation of photoexcited carriers, compared with PL performance from individual perovskite (Figure S5b, Supporting Information).

Next, we studied the response time of PdSe₂/perovskite device, which is an important criterion for optical communication application.^[51] To record the response speed, an NIR laser diode driven by a function generator was used as the pulsed

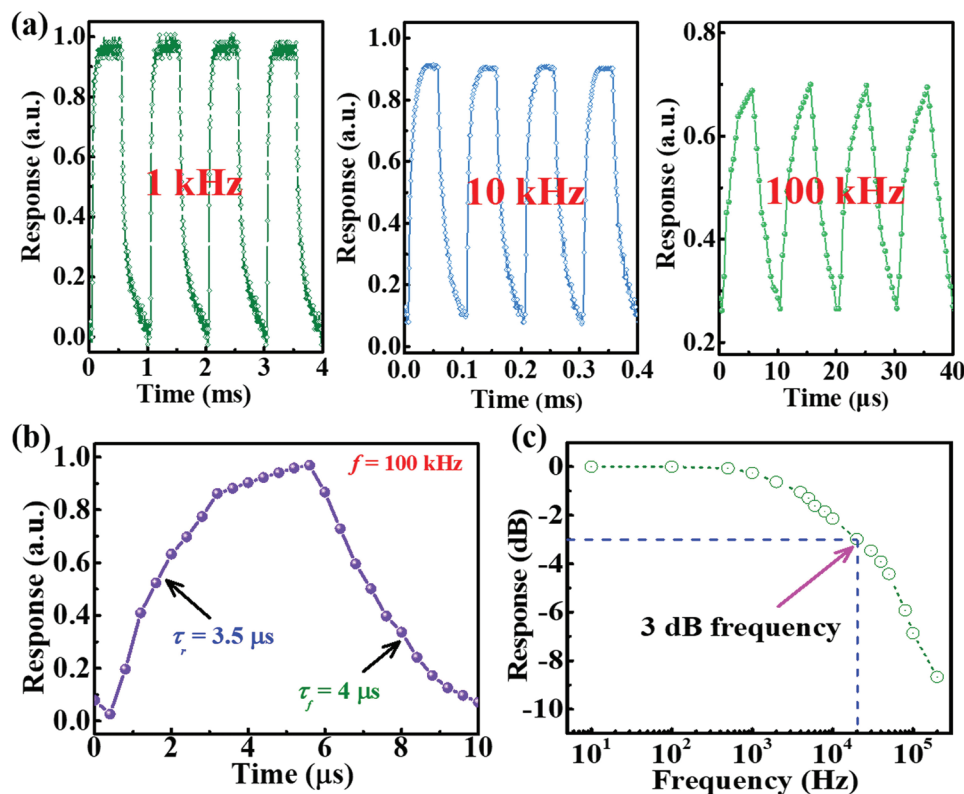


Figure 5. a) Photoresponse of the PdSe₂/perovskite Schottky junction device under pulsed light illumination with frequency of 1, 10, and 100 kHz. b) A single enlarged curve of photoresponse for calculating rise/fall time. c) Normalized response versus varying frequency, showing 3 dB cutoff frequency of ≈ 20.1 kHz.

Table 1. Comparison of the performance parameters of the PdSe₂/perovskite detector with similar heterostructure photodetectors.

Device structure	τ_r/τ_f	$I_{\text{light}}/I_{\text{dark}}$	D^* (Jones)	Self-powered	λ [μm]	Ref.
PdSe ₂ /FA _{0.85} Cs _{0.15} PbI ₃	3.5/4 μs	≈10 ⁴	≈10 ¹³	Yes	0.2–1.5	This work
MoS ₂ /MAPbI ₃	10.7/6.2 s	10	≈10 ¹⁰	No (20 V)	0.52–0.85	[16]
WS ₂ /CH ₃ NH ₃ PbI ₃	2.7/7.5 ms	≈10 ⁴	≈10 ¹²	No (5 V)	0.47–0.627	[24]
PdSe ₂ /MoS ₂	74.5/93.1 ms	<10	≈10 ⁹	No (1 V)	0.45–10.6	[32]
PdSe ₂ FET	220/220 ms	<10	≈10 ⁹	No (1 V)	–	[33]
WSe ₂ /CH ₃ NH ₃ PbI ₃	–	–	≈10 ¹¹	No (2 V)	0.2–0.9	[59]
MoS ₂ /CsPbBr ₃	0.72/1.01 ms	–	≈10 ¹⁰	No (10 V)	0.35–0.65	[60]

illuminating source. Figure 5a displays the response of detector to pulsed signal with frequency of 1, 10, and 100 kHz, signifying that the as-assembled Schottky junction device can work properly with excellent stability and reproducibility at very high frequency. Based on the definition of response speed, the rise/fall time (τ_r/τ_f) is determined to be 3.5/4 μs from the single magnified response curve at 100 kHz (Figure 5b).^[52–55] Such a fast response speed is correlated to the built-in potential at the interface of PdSe₂/perovskite and the outstanding electrical properties of PdSe₂, which will be discussed in detail later. Figure 5c shows the normalized response versus input pulsed frequency, from which the 3 dB bandwidth of the Schottky junction device is estimated to be ≈20.1 kHz. Such 3 dB frequency is much higher than that of SnS₂/PbS hybrid detector (≈50 Hz),^[56] and PtSe₂/CdTe (≈6.2 kHz),^[57] but slightly lower than that of Sn-containing perovskite NIR photodetector (≈100 kHz).^[58] **Table 1** summarizes the main device parameters of the PdSe₂/perovskite detector and other devices with similar configurations. It is obvious that the response speed, on/off ratio, and specific detectivity are better than not only PdSe₂ based devices, but also other photodetectors composed of 2D materials.^[59,60] Such good results can be mainly attributed to the following three factors: 1) The high quality PdSe₂/perovskite interface. The relatively low amounts of defects can greatly reduce the recombination activity, which will greatly increase responsivity as well as specific detectivity. 2) The strong built-in potential formed by Schottky junction. The built-in electric field is highly beneficial for the fast separation and transportation of photogenerated electron–hole carriers, giving rise to fast photoresponse. 3) The relatively good carrier transport property 2D PdSe₂. According to our calculation (Figure S6, Supporting Information), the hole mobility is calculated to be 4.75 cm² V⁻¹ s⁻¹, which enables quick drift of charge carriers under the built-in potential, leading to short carrier transit times and then quick response speed.

As an important optoelectronic device, infrared image sensor that has been widely applied in digital systems, thermometer, surveillance camera, and temperature measurement, has stimulated increasing research interest.^[61,62] To further explore the possibility of the present PdSe₂/perovskite device for infrared image sensing, an image sensing analysis setup based on individual PdSe₂/perovskite device was developed, as displayed in **Figure 6a**. For the sake of convenience, five homemade metal masks (“P,” “O,” “L,” “Y,” and “U”) were placed between laser illumination and device sequentially (See the characters of “POLYU” as an abbreviation for our university of “The Hong Kong Polytechnic University”). The measured dark current and

photocurrent, corresponding to the background noise level and light intensity level at each pixel, respectively, were incorporated into a plot and then generated an obvious 2D contrast mapping profile. As illustrated in **Figure 6b**, for all five characters, only the pixels projected by 808 nm irradiation exhibited sizeable photocurrent of around 0.05 μA, while the rest of the area displayed very weak dark current, suggesting that all the shape of characters “P,” “O,” “L,” “Y,” and “U” can be clearly observed in current contrast mapping, with decent resolution. This image sensing ability, along with the pronounced response speed and high specific detectivity render the present device highly promising for future optoelectronic devices and systems application.

3. Conclusion

In conclusion, we have developed a fast, self-powered, highly polarization-sensitive, and broadband detector by integrating 2D PdSe₂ with Cs-doped FAPbI₃, which can detect broadband light illumination from 200 to 1550 nm. Further photoresponse characterization reveals that the present device exhibits superior performance in terms of a high on/off ratio (≈10⁴), a large responsivity (313 mA W⁻¹) and specific detectivity (≈10¹³ Jones), and a good polarization sensitivity (≈6.04), together with a fast response speed of 3.5/4 μs. In addition to above excellent features, with the help of optical-assisted displacement platform, the five simple images (e.g., “P,” “O,” “L,” “Y,” and “U”) produced 808 nm can be easily recorded by our present detector. Therefore, it is expected that such a simple, and reliable PdSe₂/perovskite Schottky junction photodetector will show great potential for hybrid optoelectronic systems.

4. Experimental Section

Materials Synthesis and Characterization: The large-area PdSe₂ films were synthesized via the simple selenization process, as demonstrated in detail in previous studies.^[37] In brief, ≈7 nm Pd layer was deposited on SiO₂/Si substrate via magnetron sputtering system. Subsequently, the as-prepared Pd thin films were transformed to PdSe₂ in tube furnace with Pd coated SiO₂/Si substrate heated up to 480 °C at center place and Se powder heated up to 220 °C in upstream side of furnace. The Cs-doped FAPbI₃ (FA_{0.85}Cs_{0.15}PbI₃) perovskite films were prepared based on modified approach previously reported.^[21] The original solution for synthesizing perovskite was prepared by adding 461 mg PbI₂ (Aldrich, 99%), 38.9 mg CsI (Aldrich, 99.9%), and 145 mg HC(NH₂)₂I (FAI) (Aldrich, 99.5%) into a mixed solvent consist of 800 μL of *N,N*-dimethylformamide (99.8%) and 200 μL of dimethyl sulfoxide (>99.9%) and stirred at 80 °C

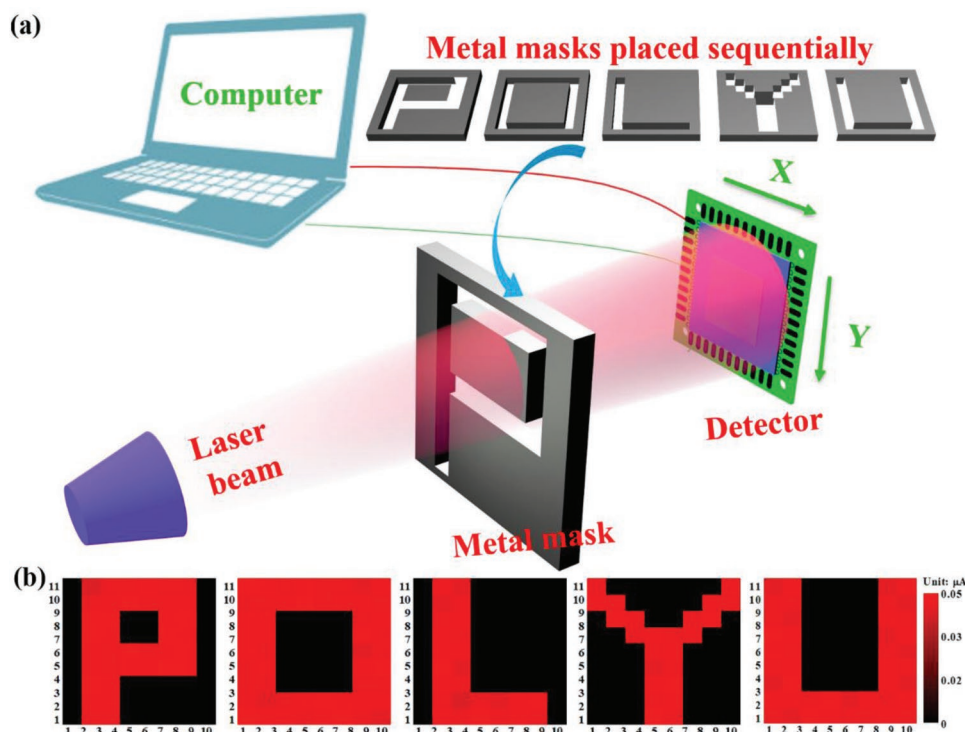


Figure 6. a) Schematic diagram of the experimental setup for detector to realize 808 nm near infrared imaging sensing. b) The corresponding 2D current mapping of characters “P,” “O,” “L,” “Y,” and “U” produced by 808 nm illumination.

for 1 h. Then, as-prepared precursor solution was spin coated onto substrate under 4000 rpm and postannealed at 140 °C for 15 min to achieve Cs-doped perovskite films.

The morphology of Cs-doped FAPbI₃ perovskite was investigated by SEM (JEOL Model JSM-6490). The XRD patterns of perovskite films were carried out to study its crystallinity in a RigakuSmartLab X-ray diffractometer. The topography of as-synthesized PdSe₂ samples was studied by AFM (Benyuan Nanotech Com, CSPM-4000). Using a field emission transmission electron microscope instrument (JEOL model JEM-2100F) with an energy-dispersive spectrometer, the chemical composition and crystal structure of PdSe₂ were well investigated. The Raman spectrum and mapping of PdSe₂ sample were performed by a HORIBA Raman spectrometer equipped with a 488 nm argon ion laser. The PL spectrum of perovskite and PdSe₂/perovskite hybrid were probed by PL system (Edinburgh Photoluminescence).

Device Fabrication and Analysis: The PdSe₂/perovskite Schottky junction device was fabricated by the one-step spin-coating method. In short, the perovskite solution was carefully spin coated onto prepatterned substrate to cover exposed parts of PdSe₂ sample. The overlapped region is effective area for PdSe₂/perovskite Schottky junction. Parallel Au electrodes (\approx 50 nm) for perovskite and PdSe₂ were prepared via magnetron sputtering using homemade shadow mask. The photoelectronic characteristics carried out using a semiconductor analysis system (Keithley 4200-SCS) together with several lasers diodes with wavelength of 265, 365, 650, 808, 1310, and 1550 nm. To record response speed, the pulsed light signal was provided by laser diode driven by a signal generator (Tektronix, TDS2022B), and an oscilloscope (Tektronix, TDS2012B) was used to record the output photoresponse. For normalized spectral response study, the monochromatic light was generated by a Xe lamp (CEL-HXF300) equipped with a monochromator (Zolix Instruments, Omni-nx I).

Supporting Information

Supporting Information is available from the Wiley Online Library or from the author.

Acknowledgements

L.-H.Z. and Q.-M.C. contributed equally to this work. This work was financially supported by the Research Grants Council of Hong Kong, China (Project No. GRF 152093/18E PolyU B-Q65N), PolyU grants (1-ZVGH), and National Natural Science Foundation of China (No. 61605174).

Conflict of Interest

The authors declare no conflict of interest.

Keywords

image sensors, palladium diselenide, perovskites, photodetectors, polarization-sensitive

Received: May 14, 2019

Revised: July 10, 2019

Published online: August 7, 2019

- [1] W. Deng, L. Huang, X. Xu, X. Zhang, X. Jin, S. T. Lee, J. Jie, *Nano Lett.* **2017**, *17*, 2482.
- [2] L. Dou, Y. M. Yang, J. You, Z. Hong, W. H. Chang, G. Li, Y. Yang, *Nat. Commun.* **2014**, *5*, 5404.
- [3] Y. Wang, R. Fullon, M. Acerce, C. E. Petoukhoff, J. Yang, C. Chen, S. Du, S. K. Lai, S. P. Lau, D. Voiry, D. O’Carroll, G. Gupta, A. D. Mohite, S. Zhang, H. Zhou, M. Chhowalla, *Adv. Mater.* **2017**, *29*, 1603995.
- [4] Y. Lee, J. Kwon, E. Hwang, C. H. Ra, W. J. Yoo, J. H. Ahn, J. H. Park, J. H. Cho, *Adv. Mater.* **2015**, *27*, 41.

- [5] S. Chen, C. Teng, M. Zhang, Y. Li, D. Xie, G. Shi, *Adv. Mater.* **2016**, *28*, 5969.
- [6] Z. Shi, Y. Li, Y. Zhang, Y. Chen, X. Li, D. Wu, T. Xu, C. Shan, G. Du, *Nano Lett.* **2017**, *17*, 313.
- [7] B. Zhao, S. Bai, V. Kim, R. Lamboll, R. Shivanna, F. Auras, J. M. Richter, L. Yang, L. Dai, M. Alsari, X.-J. She, L. Liang, J. Zhang, S. Lilliu, P. Gao, H. J. Snaith, J. Wang, N. C. Greenham, R. H. Friend, D. Di, *Nat. Photonics* **2018**, *12*, 783.
- [8] Z. Gu, K. Wang, W. Sun, J. Li, S. Liu, Q. Song, S. Xiao, *Adv. Opt. Mater.* **2016**, *4*, 472.
- [9] G. Xing, N. Mathews, S. S. Lim, N. Yantara, X. Liu, D. Sabba, M. Gratzel, S. Mhaisalkar, T. C. Sum, *Nat. Mater.* **2014**, *13*, 476.
- [10] H. Tsai, W. Nie, J. C. Blancon, C. C. Stoumpos, R. Asadpour, B. Harutyunyan, A. J. Neukirch, R. Verduzco, J. J. Crochet, S. Tretiak, L. Pedesseau, J. Even, M. A. Alam, G. Gupta, J. Lou, P. M. Ajayan, M. J. Bedzyk, M. G. Kanatzidis, *Nature* **2016**, *536*, 312.
- [11] Y. Li, Z. Shi, L. Lei, Z. Ma, F. Zhang, S. Li, D. Wu, T. Xu, X. Li, C. Shan, G. Du, *ACS Photonics* **2018**, *5*, 2524.
- [12] Y. Fang, Q. Dong, Y. Shao, Y. Yuan, J. Huang, *Nat. Photonics* **2015**, *9*, 679.
- [13] X. Yu, P. Yu, D. Wu, B. Singh, Q. Zeng, H. Lin, W. Zhou, J. Lin, K. Suenaga, Z. Liu, Q. J. Wang, *Nat. Commun.* **2018**, *9*, 1545.
- [14] X. Yu, Y. Li, X. Hu, D. Zhang, Y. Tao, Z. Liu, Y. He, M. A. Haque, Z. Liu, T. Wu, Q. J. Wang, *Nat. Commun.* **2018**, *9*, 4299.
- [15] X. Yu, Z. Dong, J. K. W. Yang, Q. J. Wang, *Optica* **2016**, *3*, 979.
- [16] D. H. Kang, S. R. Pae, J. Shim, G. Yoo, J. Jeon, J. W. Leem, J. S. Yu, S. Lee, B. Shin, J. H. Park, *Adv. Mater.* **2016**, *28*, 7799.
- [17] Z. Zheng, F. Zhuge, Y. Wang, J. Zhang, L. Gan, X. Zhou, H. Li, T. Zhai, *Adv. Funct. Mater.* **2017**, *27*, 1703115.
- [18] J. Q. Liu, Y. Gao, G. A. Wu, X. W. Tong, C. Xie, L. B. Luo, L. Liang, Y. C. Wu, *ACS Appl. Mater. Interfaces* **2018**, *10*, 27850.
- [19] H. Deng, D. Dong, K. Qiao, L. Bu, B. Li, D. Yang, H. E. Wang, Y. Cheng, Z. Zhao, J. Tang, H. Song, *Nanoscale* **2015**, *7*, 4163.
- [20] W. Deng, X. Zhang, L. Huang, X. Xu, L. Wang, J. Wang, Q. Shang, S. T. Lee, J. Jie, *Adv. Mater.* **2016**, *28*, 2201.
- [21] F.-X. Liang, J.-Z. Wang, Z.-X. Zhang, Y.-Y. Wang, Y. Gao, L.-B. Luo, *Adv. Opt. Mater.* **2017**, *5*, 1700654.
- [22] Y. Yu, Y. Zhang, Z. Zhang, H. Zhang, X. Song, M. Cao, Y. Che, H. Dai, J. Yang, J. Wang, H. Zhang, J. Yao, *J. Phys. Chem. Lett.* **2017**, *8*, 445.
- [23] X. Zou, Y. Li, G. Tang, P. You, F. Yan, *Small* **2019**, *15*, 1901004.
- [24] C. Ma, Y. Shi, W. Hu, M. H. Chiu, Z. Liu, A. Bera, F. Li, H. Wang, L. J. Li, T. Wu, *Adv. Mater.* **2016**, *28*, 3683.
- [25] F. H. Koppens, T. Mueller, P. Avouris, A. C. Ferrari, M. S. Vitiello, M. Polini, *Nat. Nanotechnol.* **2014**, *9*, 780.
- [26] L. Wang, L. Huang, W. C. Tan, X. Feng, L. Chen, X. Huang, K.-W. Ang, *Small Methods* **2018**, *2*, 1700294.
- [27] X. Zhou, X. Hu, J. Yu, S. Liu, Z. Shu, Q. Zhang, H. Li, Y. Ma, H. Xu, T. Zhai, *Adv. Funct. Mater.* **2018**, *28*, 1706587.
- [28] H. C. Cheng, G. Wang, D. Li, Q. He, A. Yin, Y. Liu, H. Wu, M. Ding, Y. Huang, X. Duan, *Nano Lett.* **2016**, *16*, 367.
- [29] Z. X. Zhang, L. H. Zeng, X. W. Tong, Y. Gao, C. Xie, Y. H. Tsang, L. B. Luo, Y. C. Wu, *J. Phys. Chem. Lett.* **2018**, *9*, 1185.
- [30] A. D. Oyedele, S. Yang, L. Liang, A. A. Poretzky, K. Wang, J. Zhang, P. Yu, P. R. Pudasaini, A. W. Ghosh, Z. Liu, C. M. Rouleau, B. G. Sumpter, M. F. Chisholm, W. Zhou, P. D. Rack, D. B. Geohegan, K. Xiao, *J. Am. Chem. Soc.* **2017**, *139*, 14090.
- [31] W. Lei, S. Zhang, G. Heymann, X. Tang, J. Wen, X. Zheng, G. Hu, X. Ming, *J. Mater. Chem. C* **2019**, *7*, 2096.
- [32] M. Long, Y. Wang, P. Wang, X. Zhou, H. Xia, C. Luo, S. Huang, G. Zhang, H. Yan, Z. Fan, X. Wu, X. Chen, W. Lu, W. Hu, *ACS Nano* **2019**, *13*, 2511.
- [33] Q. Liang, Q. Wang, Q. Zhang, J. Wei, S. X. Lim, R. Zhu, J. Hu, W. Wei, C. Lee, C. Sow, W. Zhang, A. T. S. Wee, *Adv. Mater.* **2019**, *31*, 1807609.
- [34] W. L. Chow, P. Yu, F. Liu, J. Hong, X. Wang, Q. Zeng, C. H. Hsu, C. Zhu, J. Zhou, X. Wang, J. Xia, J. Yan, Y. Chen, D. Wu, T. Yu, Z. Shen, H. Lin, C. Jin, B. K. Tay, Z. Liu, *Adv. Mater.* **2017**, *29*, 1602969.
- [35] J. Sun, H. Shi, T. Siegrist, D. J. Singh, *Appl. Phys. Lett.* **2015**, *107*, 153902.
- [36] L.-H. Zeng, S.-H. Lin, Z.-J. Li, Z.-X. Zhang, T.-F. Zhang, C. Xie, C.-H. Mak, Y. Chai, S. P. Lau, L.-B. Luo, Y. H. Tsang, *Adv. Funct. Mater.* **2018**, *28*, 1705970.
- [37] L.-H. Zeng, D. Wu, S.-H. Lin, C. Xie, H.-Y. Yuan, W. Lu, S. P. Lau, Y. Chai, L.-B. Luo, Z.-J. Li, Y. H. Tsang, *Adv. Funct. Mater.* **2019**, *29*, 1806878.
- [38] X. Xia, W. Wu, H. Li, B. Zheng, Y. Xue, J. Xu, D. Zhang, C. Gao, X. Liu, *RSC Adv.* **2016**, *6*, 14792.
- [39] Y. Xue, Y. Zhang, Y. Liu, H. Liu, J. Song, J. Sophia, J. Liu, Z. Xu, Q. Xu, Z. Wang, J. Zheng, Y. Liu, S. Li, Q. Bao, *ACS Nano* **2016**, *10*, 573.
- [40] Z. Wang, Q. Li, F. Besenbacher, M. Dong, *Adv. Mater.* **2016**, *28*, 10224.
- [41] J. Lu, A.-X. Wei, Y. Zhao, L. Tao, Y. Yang, Z. Zheng, H. Wang, D. Luo, J. Liu, L. Tao, *ACS Photonics* **2018**, *5*, 4912.
- [42] M. S. Choi, D. Qu, D. Lee, X. Liu, K. Watanabe, T. Taniguchi, W. J. Yoo, *ACS Nano* **2014**, *8*, 9332.
- [43] P. Xiao, J. Mao, K. Ding, W. Luo, W. Hu, X. Zhang, X. Zhang, J. Jie, *Adv. Mater.* **2018**, *30*, 1801729.
- [44] L. H. Zeng, S. H. Lin, Z. Lou, H. Yuan, H. Long, Y. Li, W. Lu, S. P. Lau, D. Wu, Y. H. Tsang, *NPG Asia Mater.* **2018**, *10*, 352.
- [45] W. Y. Kong, G. A. Wu, K. Y. Wang, T. F. Zhang, Y. F. Zou, D. D. Wang, L. B. Luo, *Adv. Mater.* **2016**, *28*, 10725.
- [46] E. Wu, D. Wu, C. Jia, Y. Wang, H. Yuan, L. Zeng, T. Xu, Z. Shi, Y. Tian, X. Li, *ACS Photonics* **2019**, *6*, 565.
- [47] L. H. Zeng, M. Z. Wang, H. Hu, B. Nie, Y. Q. Yu, C. Y. Wu, L. Wang, J. G. Hu, C. Xie, F. X. Liang, L. B. Luo, *ACS Appl. Mater. Interfaces* **2013**, *5*, 9362.
- [48] S. Mukherjee, K. Das, S. Das, S. K. Ray, *ACS Photonics* **2018**, *5*, 4170.
- [49] L. Gao, K. Zeng, J. Guo, C. Ge, J. Du, Y. Zhao, C. Chen, H. Deng, Y. He, H. Song, G. Niu, J. Tang, *Nano Lett.* **2016**, *16*, 7446.
- [50] Z. Zhou, M. Long, L. Pan, X. Wang, M. Zhong, M. Blei, J. Wang, J. Fang, S. Tongay, W. Hu, J. Li, Z. Wei, *ACS Nano* **2018**, *12*, 12416.
- [51] X. Yuan, L. Tang, S. Liu, P. Wang, Z. Chen, C. Zhang, Y. Liu, W. Wang, Y. Zou, C. Liu, N. Guo, J. Zou, P. Zhou, W. Hu, F. Xiu, *Nano Lett.* **2015**, *15*, 3571.
- [52] Z. Lou, L. Zeng, Y. Wang, D. Wu, T. Xu, Z. Shi, Y. Tian, X. Li, Y. H. Tsang, *Opt. Lett.* **2017**, *42*, 3335.
- [53] R. Zhuo, L. Zeng, H. Yuan, D. Wu, Y. Wang, Z. Shi, T. Xu, Y. Tian, X. Li, Y. H. Tsang, *Nano Res.* **2019**, *12*, 183.
- [54] R. Zhuo, Y. Wang, D. Wu, Z. Lou, Z. Shi, T. Xu, J. Xu, Y. Tian, X. Li, *J. Mater. Chem. C* **2018**, *6*, 299.
- [55] Y. Li, Z. Shi, L. Lei, F. Zhang, Z. Ma, D. Wu, T. Xu, Y. Tian, Y. Zhang, G. Du, C. Shan, X. Li, *Chem. Mater.* **2018**, *30*, 6744.
- [56] L. Gao, C. Chen, K. Zeng, C. Ge, D. Yang, H. Song, J. Tang, *Light: Sci. Appl.* **2016**, *5*, e16126.
- [57] D. Wu, Y. Wang, L. Zeng, C. Jia, E. Wu, T. Xu, Z. Shi, Y. Tian, X. Li, Y. H. Tsang, *ACS Photonics* **2018**, *5*, 3820.
- [58] X. Xu, C.-C. Chueh, P. Jing, Z. Yang, X. Shi, T. Zhao, L. Y. Lin, A. K. Y. Jen, *Adv. Funct. Mater.* **2017**, *27*, 1701053.
- [59] J. Lu, A. Carvalho, H. Liu, S. X. Lim, A. H. Castro Neto, C. H. Sow, *Angew. Chem., Int. Ed.* **2016**, *55*, 11945.
- [60] X. Song, X. Liu, D. Yu, C. Huo, J. Ji, X. Li, S. Zhang, Y. Zou, G. Zhu, Y. Wang, M. Wu, A. Xie, H. Zeng, *ACS Appl. Mater. Interfaces* **2018**, *10*, 2801.
- [61] P. Wang, S. Liu, W. Luo, H. Fang, F. Gong, N. Guo, Z. G. Chen, J. Zou, Y. Huang, X. Zhou, J. Wang, X. Chen, W. Lu, F. Xiu, W. Hu, *Adv. Mater.* **2017**, *29*, 1604439.
- [62] X. Yuan, L. Tang, P. Wang, Z. Chen, Y. Zou, X. Su, C. Zhang, Y. Liu, W. Wang, C. Liu, F. Chen, J. Zou, P. Zhou, W. Hu, F. Xiu, *Nano Res.* **2015**, *8*, 3332.